



Published in final edited form as:

Nat Commun. ; 5: 5624. doi:10.1038/ncomms6624.

Ligand engaged TCR is triggered by Lck not associated with CD8 coreceptor

Javier Casas^{1,2}, Joanna Brzostek^{1,2}, Veronika I. Zarnitsyna³, Jin-sung Hong⁴, Qianru Wei¹, John A.H. Hoerter², Guo Fu², Jeanette Ampudia², Rose Zamoyska⁵, Cheng Zhu^{3,4}, and Nicholas R.J. Gascoigne^{1,2,*}

¹Department of Microbiology, Yong Loo Lin School of Medicine, National University Health System, National University of Singapore, 5 Science Drive 2, Singapore 117545

²Department of Immunology and Microbial Sciences, The Scripps Research Institute, 10550 N. Torrey Pines Rd., La Jolla, CA, 92037 USA

³Wallace H Coulter Department of Biomedical Engineering, Georgia Institute of Technology and Emory University, Atlanta, GA 30332, USA

⁴George W Woodruff School of Mechanical Engineering, Georgia Institute of Technology and Emory University, Atlanta, GA 30332, USA

⁵Institute of Immunology and Infection Research, University of Edinburgh, Edinburgh, Scotland, UK

Abstract

The earliest molecular events in T cell recognition have not yet been fully described, and the initial T cell receptor (TCR) triggering mechanism remains a subject of controversy. Here, using TIRF/FRET microscopy, we observe a two-stage interaction between TCR, CD8, and MHCp. There is an early (within seconds) interaction between CD3 ζ and the coreceptor CD8 that is independent of the binding of CD8 to MHC, but that requires CD8 association with Lck. Later (several minutes) CD3 ζ -CD8 interactions require CD8-MHC binding. Lck can be found free or bound to the coreceptor. This work indicates that the initial TCR triggering event is induced by free Lck.

Users may view, print, copy, and download text and data-mine the content in such documents, for the purposes of academic research, subject always to the full Conditions of use:http://www.nature.com/authors/editorial_policies/license.html#terms

*Correspondence should be addressed to N.R.J.G. (micnrjg@nus.edu.sg).

Present addresses: V.I.Z., Department of Biology, Emory University, Atlanta, GA; J.A.H.H., Genomics Institute of the Novartis Research Foundation, San Diego, CA 92121, USA; G.F., State Key Laboratory of Cellular Stress Biology, Innovation Center for Cell Biology, School of Life Sciences, Xiamen University, Fujian 361102, China; J.A., Takeda Pharmaceutical Company, San Diego, CA 92121, USA.

Author Contributions

J.C. performed most of the experiments. J.B., J.A.H.H., G.F., Q.W. and J.A. generated antigen presenting cell lines, constructs and mutants. V.Z. and J.H. performed adhesion frequency assays. J.C., J.B., V.Z., and J.H. analyzed data; J.C. and N.R.J.G. designed the project with help and insight from J.C., J.B. and C.Z.; J.C. and N.R.J.G. wrote the manuscript.

Introduction

Antigen recognition by the T cell receptor (TCR) is the first step in T cell activation, and the paramount event for their development and functions. At the start of the signaling cascade, the immunoreceptor tyrosine-based activation motifs (ITAMs) of the CD3 signaling subunits of the TCR are phosphorylated by the Src-family kinase (SFK) Lck and, to a lesser extent, Fyn, and then bound by another kinase called ZAP70¹⁻³. After ZAP70 binds to CD3, the coreceptors CD4 or CD8, which are associated with the SFK Lck, become associated with the TCR-CD3 complex and bind to major histocompatibility complex (MHC). This stabilizes the TCR-MHC-peptide (MHCp) interaction (at least in the case of CD8⁴), and Lck continues the phosphorylation of CD3 elements, ZAP70 and the many other downstream targets. Freshly isolated T cells, but not T cell lines, show partial phosphorylation of CD3 ζ with bound but non-phosphorylated ZAP70⁵. This condition is thought to represent stimulation by self MHCp *in vivo*⁶.

Although TCR triggering has been extensively studied, the precise timing of signals downstream of the TCR is as yet poorly understood. TCR microclusters, in which signaling occurs, form at the immunological synapse (IS) within seconds of MHCp recognition⁷. Using MHC complexes containing an antigenic peptide that is biologically inert until exposed to ultraviolet (UV) light, Huse and co-workers developed a high resolution temporal analysis of signaling. Phosphorylation of the adaptor molecule LAT was observed within 4 s, and diacylglycerol production and calcium flux was observed after 6–7s (Ref.⁸). A recent biophysical study on TCR and CD8 binding to MHCp demonstrated that the initial binding of TCR to MHCp induces, in a SFK-dependent manner, the binding of CD8 to the MHCp⁹, leading to the question of how the TCR-CD3 complex is initially phosphorylated by an SFK before CD8 and the associated Lck have been recruited to the TCR-CD3 complex.

CD8 coreceptor is expressed on cytotoxic T lymphocytes and their double positive (DP) thymic progenitors, where its main function is to augment the sensitivity and response of T cells to cognate MHCp ligands^{4,10}. It is generally accepted that the ability of the coreceptor to enhance T-cell responses is due to two main effects: (i) Binding of CD8 to MHC class I (MHCI) molecules helps stabilize weak TCR-MHCp interactions; and (ii) the recruitment of Lck, which is bound to the cytoplasmic tail of coreceptor, to the TCR complex upon coreceptor binding to the MHC, thereby enhancing the initiation of TCR signaling^{4,11}. Lck consists of N-terminal sequences that mediate its myristoylation, palmitoylation and association with co-receptors, followed by SH3, SH2 and tyrosine kinase domains, and C-terminal negative regulatory domain¹². Lck can be found either free in the cytosol¹³, anchored to the plasma membrane through myristoylation and palmitoylation, or associated with the CD8 or CD4 coreceptors through a “zinc-clasp” structure¹⁴. Lck activity is largely controlled by the equilibrium between phosphorylation and dephosphorylation at a C-terminal inhibitory tyrosine (Y⁵⁰⁵) and an activating tyrosine in the catalytic domain (Y³⁹⁴)². Relatively high amounts (up to ~40%) of constitutively active pY³⁹⁴-Lck are present in resting T cells and thymocytes¹⁵ suggesting an important role of spatial organization of Lck and TCR in regulation of TCR triggering¹⁶. Lck also has a poorly understood kinase-independent function¹⁷. Chimeric proteins formed by CD4 fused to Lck

with deleted kinase domain were shown to be more efficient at supporting full activation of a CD4-dependent T cell hybridoma than the full length chimeric fusion protein¹⁸. This kinase-independent activity was largely dependent on intact SH2, SH3 domains as well as presence of intact endogenous Lck in the CD4 deficient T cell hybridoma¹⁹. Importantly, CD8 α -Lck kinase-dead fusion protein could reconstitute thymic development in MHC I restricted TCR transgenic CD8 α -deficient mice²⁰, suggesting that one of the functions of Lck is to serve as an adaptor molecule that regulates the interactions of the coreceptor with MHC and TCR¹⁸.

Previously, we used Forster resonance energy transfer (FRET) microscopy in live and fixed cells to investigate the interaction of CD4 or CD8 with TCR, using CD3 ζ -CFP as FRET donor and CD4-YFP or CD8 β -YFP as FRET acceptors²¹⁻²⁴. We showed that the coreceptors interact with the TCR only after recognition of antigenic MHCp, but CD8 can be recruited to the immunological synapse independently of the sequence of peptide presented on MHC²¹⁻²³. We also found that the strength of the interaction measured by FRET between the TCR complex and CD8 corresponded closely to the strength of T cell activation by particular peptides, and that differences in FRET kinetics during recognition of different MHCp ligands correlated closely to the ability of a particular ligand to induce positive or negative selection in thymocytes^{24,25}. However, the temporal resolution of these studies was limited, and they could not provide more detailed information about the sequence of molecular events during TCR triggering. We therefore decided to look more closely at the earliest stages of the interaction using the higher spatial and temporal resolution afforded by total internal reflection (TIRF) microscopy of T cells interacting with supported lipid bilayers as model antigen presenting surfaces²⁶. In the present study we show conclusively that TCR triggering occurs in two distinct stages: early phosphorylation of TCR-CD3 by Lck that is not associated with coreceptor leading to MHC-independent association between CD8 and TCR-CD3, followed later by MHC-dependent CD3-CD8 interaction^{3,9,17}. The free, active Lck initiates TCR-CD3 complex phosphorylation; whereas the coreceptor associated Lck acts mainly as an adaptor molecule, recruiting CD8 to the phosphorylated TCR-CD3 complex through direct binding to phospho-CD3 or to phospho-ZAP70 associated with phosphorylated CD3.

Results

Antigen induced CD8 β -CD3 ζ interaction

We first assessed the relationship between CD8 recruitment to the immune synapse and its ability to bind to MHCp by analyzing the synapses formed between OT-I T cell hybridomas expressing CD3 ζ -CFP and CD8 α,β -YFP (hybridoma cell line hence referred to as OT-I.ZC.8 β Y) cells²³, and a surrogate antigen presenting cell line: CHO cells expressing either inducible wild-type scH-2K^b-OVA or a D²²⁷K/E²²⁹K mutant that cannot bind to CD8 (scH-2-K^b-OVA-CD8_{mut}). These sc-MHCI constructs were described previously²⁷. The OT-I TCR recognizes the agonist OVA peptide (SIINFEKL) with high affinity, but not the VSV peptide (RGYVYQGL), when either is presented by H-2K^b. We compared the intensity of CD8 β -YFP fluorescence in the immune synapse, showing that the CD8 recruitment itself

was not solely a result of TCR recognition of MHCp, but instead was driven by the CD8-MHCI interaction (Fig. 1a), as indicated by our earlier work^{23,28}.

Because of the differences in timing between our previous measurements of FRET between TCR and coreceptors^{21,23,24}, and other's analyses of early signaling events during T cell antigen recognition^{8,9}, we decided to further characterize the TCR-CD8 interaction. The interaction between two molecules can be studied using Forster Resonance Energy Transfer (FRET), which occurs only between molecules separated by 10 nm or less. After donor excitation, FRET leads, due to the energy transfer, to decreased donor fluorescence and increased acceptor fluorescence²⁹. We allowed CHO cells expressing either sc-H-2K^b-OVA or sc-H-2K^b-VSV to settle in a 37°C heated chamber before the addition of OT-I.ZC.8βY cells. We monitored the interaction between CD3ζ-CFP and CD8β-YFP by live FRET efficiency (*E*-FRET) imaging during the process of antigen recognition^{21,30}. After stimulation with sc-H-2K^b-OVA expressing cells, both CD3ζ-CFP and CD8β-YFP were recruited to the synapse, where the FRET signal between CD3ζ-CFP and CD8β-YFP began to increase strongly about 5 min after the beginning of the APC-T cell interaction (Fig. 1B) until it peaked at 10 min, remaining oscillating for another 10 min and then decreasing. No detectable FRET was found at any time when the T cells interacted with the non-stimulatory sc-H2K^b-VSV-expressing CHO cells. These results agreed with previous studies from this lab^{23,24}, but we considered it likely that we were underestimating the timing and the potency of the interaction due to technical limitations of the experimental setup, and to the fact that we were analyzing the average FRET efficiency over the whole synapse. During the interaction of sc-H-2K^b-OVA-expressing CHO cells with 17αβ cells (T cell hybridoma expressing OT-I TCR and CD8αβ) loaded with the Ca²⁺ fluorescent indicator Fluo-4, cytosolic Ca²⁺ concentration [Ca²⁺]_i increased at the very moment that the initiation of the interaction was observed (Fig. 1b right plot). This suggested that we were indeed missing early signaling events.

Looking closely at the FRET data in Fig.1B, we noted that there appeared to be a slight rise in the *E*-FRET signal at the time of contact between the T cell and the APC, which continued until the main *E*-FRET increase at ~5 minutes. While its significance was questionable, we hypothesized that this could represent small localized regions of TCR-CD8 interaction that were “diluted” in the analysis of the whole synapse. To improve the resolution of our imaging, we used artificial supported lipid bilayers as antigen presenting surfaces^{26,31}, imaging the immunological synapse between the T cell and the bilayer presenting H-2K^b-peptide complex as well as ICAM-1 (Fig. 2a). We used a TIRF microscopy system that allowed us to increase spatial resolution by exciting only the fluorophores immediately adjacent to the glass-oil interface ($z=100$ nm), in other words, imaging the immune synapse. The bilayers were fully functional as surrogate antigen presenting surfaces, supporting full lipid motility, determined by fluorescence recovery after photobleaching (FRAP in Supplementary Fig. 1a) and antigen-specific T cell activation (determined by MHCp relocation in Supplementary Fig. 1b, Ca²⁺ flux in Supplementary Fig. 1c and total phosphotyrosine imaging in Supplementary Fig. 1d), We switched fluorophores to green and red fluorescent proteins (eGFP as donor and mCherry as acceptor) to be compatible with the TIRFM system. Thus, using a new hybridoma cell line expressing

CD3 ζ -eGFP and CD8 β -mCherry, hence referred to as OT-I.ZG.8 β R, T cells stimulated by H-2K^b-OVA bilayers we were able, not only to reproduce the kinetics of our previous results in live and fixed cells, but also to detect a weak but significant increase in FRET efficiency in the earliest time-point analyzed (1 min) (Fig. 2b, c). This FRET signal was not observed in T cells interacting with bilayers presenting the non-stimulatory H-2K^b-VSV complexes. This early FRET was observed in small localized clusters. This likely corresponds to the very early moments of antigen recognition, taking into account that it takes about 30–60 seconds for the settling cells to reach the bilayer. After this initial CD3 ζ -CD8 β interaction, a stronger interaction occurred after about 5 min. These results clearly indicate a two stage interaction process.

CD8 β -CD3 ζ interaction is a two stage process

A recent study also suggests biphasic TCR and CD8 interactions with peptides presented by MHC class I (MHCI)⁹. In the first step, TCR binds MHCp, causing SFK activity that is a pre-requisite for the second stage, when CD8 binds MHCI⁹. The CD8-MHCI interaction stabilizes the interaction between the three molecules. Thus the kinase activity of the first stage occurs before CD8 has had a chance to associate with the MHCI. Since the SFK Lck is thought to be associated with the coreceptor, the mechanism for the initial phosphorylation step is unclear³. Using a T cell hybridoma expressing OT-I TCR with CD3 ζ -eGFP, CD8 α and a S¹⁰¹A/K¹⁰³D CD8 β mutant that cannot bind to MHCI, CD8 β -MHC_{mut}-mCherry (hence referred to as OT-I.ZG.8 β -MHC_{mut}R) (Refs.^{23,28,32}). We observed an early CD3-CD8 FRET signal in T cells expressing the CD8 mutant that cannot bind to MHC, when exposed to MHCp complexes, and this FRET signal was comparable to the signal observed for T cells expressing wild-type CD8 (Fig. 3a). In contrast, CD8 unable to bind MHC class I did not interact with CD3 at 15 min, and did not enable T cell activation (Fig. 3a,b). In order to further confirm the importance of CD8 binding to MHCI for the late FRET signals, we tested the activation state of the cells (15 min) by total phospho-Tyr staining and compared total phospho-Tyr levels in cells expressing wild-type CD8 in response to wild type MHCI monomers or with chimeric monomers consisting of mouse α 1 α 2 heavy chain and human α 3 domain that cannot bind to mouse CD8 (H-2K^b-OVA-HLA-A*02:01)⁹ presented on the bilayers with cells expressing CD8 mutant that cannot bind MHCI (Fig. 3c). In addition we used primary OT-I CTL cells plus or minus CD8-blocking antibodies in bilayers presenting wild-type MHCI molecules or MHCI molecules that cannot bind CD8 (Fig. 3d). When the blocking anti-CD8 Ab was present, or in response to MHCI mutant, total phospho-Tyr activity was as low as when the non-stimulatory VSV peptide was presented (Fig. 3c, d).

Lck interaction with CD8 is necessary for initial CD8 recruitment

To test whether CD8 needed to be bound to Lck in order to interact with TCR-CD3 complex after antigen recognition, we imaged early and late FRET signals during antigen recognition by OT-I T hybridoma cells expressing CD3 ζ -eGFP, CD8 β -mCherry, and CD8 with a mutation of the intracellular CxCP motif that mediates the interaction with Lck (hence referred to as OT-I.ZG.8 α CxCP_{mut}/8 β .R). The C²²⁷KC²²⁹P motif was mutated to S²²⁷KS²²⁹P (Ref.³³). This experiment showed that the Lck-binding mutation completely abrogated the early interaction between CD3 ζ -GFP CD8 β -mCherry as well as the later phospho-Tyr signaling (Fig. 3a,b). This suggests that the Lck interaction with CD8 was

required to bring CD8 close to the TCR-CD3 complex at the early time-point. The interaction between MHCI and CD8 is strong enough to overcome this effect at later time points, as indicated by the recovery of the second interaction stage (Fig. 3a).

CD8-Lck and MHCp interactions required for 2-stage kinetics

Our FRET data strongly suggest that CD8 interactions with TCR-CD3 occur in two stages, with the early (<1 min) stage requiring CD8 binding to Lck, but not to MHC, and the late (>5min) stage requiring CD8 binding to MHC, but not to Lck. We validated the relevance of this finding using the adhesion frequency assay for analysis of two-dimensional (2D) binding described previously^{9,34,35}. In brief, an OT-I T-hybridoma cell with various combinations of transduced signaling proteins and a RBC bearing H-2K^b-OVA were aspirated by respective pipettes and driven in and out of contact with controlled area and duration. Adhesion was defined as stretching of the RBC on T cell retraction⁹. This contact-retraction cycle was repeated 50 times for a given contact duration on each cell pair. We performed 2D binding studies with the three different hybridomas expressing either wild-type CD8 molecules, or CD8 with abrogated binding to Lck or MHC. The kinetics of their interactions with K^b-OVA, were expressed as the normalized adhesion bonds $\langle n \rangle / m_{pMHC}$. Plots of $\langle n \rangle / m_{pMHC}$ of cells expressing OT-I TCR with CD3 ζ , CD8 α and CD8 β showed two-stage kinetics, whereas plots from cells expressing either CD8 α -CxCP_{mut} (Fig. 4a) or CD8 β -MHC_{mut} (Fig. 4b) showed single-stage kinetics. This confirmed that the Lck interaction with CD8 was required to bring CD8 close to the TCR, and that the CD8-MHCI interaction was responsible for the second binding stage that results in the late FRET peak.

In order to investigate TCR triggering in primary T cells, cytotoxic T lymphocytes (CTL) were prepared from OT-I TCR transgenic mouse splenocytes after activation by OVA peptide with addition of IL-2. CTL were transduced with a biosensor for CD3 ITAM phosphorylation consisting of mCherry fused to the tandem SH2 domains of ZAP70 (mCherry-tSH2(ZAP70))³⁶. In resting T cells ZAP70 is located in the cytosol but upon TCR activation it relocates to the plasma membrane through association of its SH2 domains to the phosphorylated ITAMs of the CD3 complex. This translocation can be detected by fluorescence microscopy upon T cell activation after crosslinking with anti-CD3 + anti-CD8 (Fig. 5a). Due to the optical characteristics of TIRF illumination, this sensor is extremely useful to analyze T cell activation at the immune synapse. After adding OT-I CTL expressing the mCherry-tSH2(ZAP70) biosensor to lipid bilayers presenting specific MHCp (H-2K^b-OVA), we observed consistent presence of mCherry-tSH2(ZAP70), indicating CD3 ITAM phosphorylation, in the immune synapse. With bilayers presenting the chimeric variant that cannot bind to CD8 (H-2K^b-OVA-HLA-A*02:01), early but transient accumulations of ZAP70 were noted (Fig. 5b).

When primary OT-I CTL were analyzed by western blot for specific phosphorylation of CD3 ζ and for Ca²⁺ flux, after stimulation with H-2K^b-OVA tetramer, we confirmed that the initial CD3 ζ phosphorylation and Ca²⁺ transients were high and sustained (Fig. 6). When the tetramers were unable to bind to CD8 there was only a small initial peak of CD3 ζ phosphorylation, and a Ca²⁺ flux that was not sustained over time. CD3 ζ phosphorylation was completely inhibited by addition of the SFK inhibitor PP2 (Fig. 6 and Supplementary

Fig. 3a). Together these data confirm, as expected, the importance of CD8-MHCI interaction for the stabilization of the trimolecular complex and for maintenance of the TCR signaling process. More interestingly, these data also demonstrate an initial SFK-dependent phosphorylation of ITAMs on the CD3 complex that is independent of the coreceptor binding to MHC.

A small amount of Lck is enough to phosphorylate the TCR

Several lines of evidence indicate that the initial phosphorylation of CD3 ζ ITAMs and ZAP70 is mediated by Lck and/or Fyn^{37–39}. Lck-deficient mice have stronger defects in most aspects of signaling than Fyn-deficient mice⁴⁰, yet the mechanism of the process that initiates the TCR signaling cascade is still obscure³. Therefore, we knocked-down Lck expression in OT-I primary CTLs using specific shRNA. After a decrease in Lck protein expression of about 60% we were still able to observe CD3 ζ phosphorylation to the same degree as control-treated cells after H2-K^b-OVA tetramer stimulation (Supplementary Fig. 2, 3a,e). These data suggests either that Fyn is compensating for Lck absence, or that only a small pool of the total Lck is responsible for the initial phosphorylation.

Free Lck is responsible for initial TCR-CD3 phosphorylation

Our data strongly indicate that a free, rather than coreceptor-bound, pool of Lck initiates CD3 phosphorylation. To further investigate the role of free Lck in initiation of TCR signaling, we used *Rag1*^{-/-} OT-I mice in which Lck expression was controlled by the induction of a tetracycline-responsive transgene⁴¹. These mice are on an *Lck*^{-/-} background, and induction of transgene expression with tetracycline successfully overcomes the lack of endogenous Lck, restoring normal thymopoiesis⁴¹. Withdrawal of the mice from tetracycline for at least 7 days (Lck^{OFF}) is sufficient to remove all residual protein⁴². We generated CTL from the Lck^{OFF} mice, and stimulated them with the agonist H-2K^b-OVA tetramers. In this system, where there is no Lck present in the cells, there was no detectable phosphorylation of CD3 ζ after specific OVA tetramer stimulation (Fig. 7a and Supplementary Fig. 3b). CD3 ζ phosphorylation was restored after transducing wild-type Lck into the Lck-deficient cells (Fig. 7b, left and Supplementary Fig. 3c,d). More interestingly, transducing the cells with a mutant version of the Lck protein that cannot interact with the coreceptor (C₂₀A/C₂₃A) (Ref. 43), restored substantial CD3 ζ phosphorylation. To further investigate the contribution of free Lck to TCR antigen recognition at the immune synapse, we expressed wild-type or C₂₀A/C₂₃A mutant Lck fused to mCherry or eGFP respectively in Lck^{OFF} OT-I CTLs and monitored, using TIRFM, its localization during interactions with lipid bilayers presenting H2-K^b-OVA and ICAM-1. Both wild-type (containing both free and coreceptor-bound forms) and mutant Lck pools were recruited to the immune synapse (Fig 8a), strongly suggesting that Lck that is not associated with the CD8 coreceptor contributes to TCR signal initiation at the immune synapse. In order to differentiate the timing between coreceptor-associated Lck and free membrane anchored Lck we prepared an OT-I T cell hybridoma expressing CD3 ζ -eGFP, a chimeric coreceptor formed by CD8 α -Lck-Cerulean, CD8 β -WT, and a mutant Lck-C20.23A-mCherry (OT-I.ZG.8 α LckC.8 β .LckC2023A.R). We stimulated the cells using lipid bilayers containing H-2K^b-OVA or H-2K^b-VSV monomers and ICAM-1 for less than 1 minute (early stimulation) or 2 minutes (late stimulation) and then performed colocalization analysis at the IS between free Lck and TCR, or coreceptor

associated Lck and TCR. The colocalization index when OVA was presented on the bilayer between free Lck and TCR was higher (0.72 ± 0.02) at the earliest timepoint (0 to 30 s) than the index corresponding to coreceptor associated Lck and TCR (0.54 ± 0.01), whereas there were no significant differences between the indexes at 30 to 60 s (0.51 ± 0.01 versus 0.50 ± 0.01 , respectively) or at any time point analyzed when the bilayers contained VSV (Fig 8b). These results strongly suggest that the free Lck initially interacts with TCR during antigen recognition, whereas co-receptor bound Lck is recruited to the TCR/CD3 complex at later time points.

Discussion

Early T cell signaling events such as LAT phosphorylation or calcium flux take place within a few seconds⁸. Performing higher-spatial/temporal resolution experiments using a supported lipid bilayer system as a surrogate antigen presenting surface, we have been able to image TCR-CD8 FRET in small regions within the immunological synapse. These were too localized to show a signal above the background when FRET signals were averaged over the whole synapse, explaining why they were not noticed before in regular live or fixed epifluorescence experiments²⁴. A recent study on TCR and CD8 binding to MHCp showed that there is a two stage interaction process in which first TCR interacts with MHCp and, after an SFK-mediated activity, there is a stabilization phase carried out by CD8-MHCp binding^{3,9}. This was identified using blocking antibodies against CD8 and the SFK inhibitor PP2, where only the first phase of the interaction takes place⁹.

Our new FRET/TIRF data show a small but significant increase in FRET signal within 1 minute of adding cells to the imaging chamber, followed by a second, stronger, increase after about 5 minutes. This suggests that the early FRET signal represents CD8 brought passively to the TCR by binding of Lck to phospho-CD3 or phospho-ZAP70. The later, stronger FRET was likely due to stabilization of the TCR-MHCp complex by CD8 binding to MHCI, because of the absence of induction of the FRET signal or Tyr-phosphorylation in cells expressing a mutant CD8 that cannot bind MHCI. This suggested that the interaction operative at early stages goes away over time. Moreover, when cells expressed a CD8 mutant that cannot bind Lck, there was only a low FRET signal, demonstrating that the Lck interaction with CD8 was required to bring CD8 close to the TCR. It might be possible that the interaction between MHCI and CD8 is strong enough to overcome this effect at later time points, as suggested by the recovery of the second interaction stage. These results were supported using the same biophysics approach conducted by Jiang et al. in their work⁹. Using OT-I T cell hybridomas we were able to detect a two stage interaction kinetic between TCR-CD8 and MHCp only when cells expressed wild-type CD8 molecules. When the cells expressed either the Lck-CD8 binding mutant or MHC-CD8 binding mutant, only the first stage of the interaction was detectable.

It is commonly accepted that CD8 is recruited to the signaling TCR by its MHCp interaction. However, if the CD8-MHCp interaction doesn't happen until after TCR ITAMs are phosphorylated, how is the initial CD8 recruitment produced? One possibility supported by our data is that passive diffusion would allow Lck to bind to the phosphorylated ITAMs on the TCR, or even directly to phospho-ZAP70, thus bringing any coreceptor-associated

Lck passively to the TCR. An earlier study with chimeras of CD4-Lck showed that mutation of the Lck SH2 domain in the chimera reduced the ability to restore thymopoiesis independently of the kinase activity, suggesting a protein-protein interaction role for Lck¹⁸.

Although Lck phosphorylation of TCR ITAMs is one of the earliest detected events in T cell activation, it still remains unsolved. Briefly, Lck activity is controlled by a balance between phosphorylation of two main tyrosine residues, Tyr³⁹⁴, known to promote an open active conformation, and Tyr⁵⁰⁵, known to promote a closed inactive conformation^{12,44}.

Conflicting data on this subject are available. Most traditional biochemical studies showed no changes on the phosphorylation level of Lck after TCR stimulation, so Lck could be accessible to very subtle regulatory mechanisms without the need for acute changes in Tyr⁵⁰⁵ and Tyr³⁹⁴ phosphorylation and conformational alterations, as FRET studies with an Lck sensor claimed⁴⁵. On the other hand, more fine measurements with the same sensor, analyzing its fluorescence lifetime, enabled the direct visualization of the dynamic local opening of 20% of the total amount of Lck proteins after activation of T cells with antibody against CD3, or by superantigen-loaded antigen-presenting cells⁴⁶. Nika and co-workers reported that up to 40% of total Lck present in unstimulated naïve T cells and thymocytes was constitutively active¹⁵, consistent with the data obtained with the fluorescent Lck reporter construct^{45,46}. This substantial, pre-existing pool of active Lck molecules in the membrane of resting T cells might be sufficient to mediate phosphorylation of the TCR. To address this question we have found that a mutant Lck (C₂₀A/C₂₃A) that cannot bind to CD8 was able to restore induction of TCR phosphorylation and showed a higher colocalization index with TCR after MHCp recognition than did coreceptor-associated Lck. This was similar to the effect of wild-type Lck in Lck-deficient cells after T cell stimulation. Given these findings, we propose a model in which before TCR interaction with MHCp, some Lck is associated with the plasma membrane, with some Lck also associated with CD8. Upon TCR binding to MHCp, non-CD8 bound Lck becomes associated with the TCR-CD3 complex, and phosphorylates CD3ζ ITAMs and then ZAP70 which binds to the phosphorylated CD3ζ ITAMs. The SH2 domain of CD8-bound Lck then interacts with phospho-ZAP70, pulling CD8 into proximity with the MHCp-interacting TCR^{47,48}. The extracellular immunoglobulin domains then bind to the MHCp, stabilizing the TCR-MHCp interaction.

Methods

Mice

B6 mice were bred at NUS. All experimental procedures performed in Singapore were approved by the institutional animal care and use committees of the National University of Singapore. OT-I, OT-I *Rag1*^{-/-} mice all on the B6 background were bred at The Scripps Research Institute and were maintained in accordance with the Animal Care and Use Committee of The Scripps Research Institute. OT-I *Rag1*^{-/-} Lck^{OFF} spleens were provided by Rose Zamoyska (School of Biological Sciences, University of Edinburgh). Mice of either sex were used between five and eight weeks old. Mice were age and sex matched in each experiment.

Constructs and cells

CHO cells expressing the tetracycline repressor (Invitrogen TRex) under blasticidin selection (10 µg/ml) were grown in Ham's F12 media with 10% (vol/vol) FCS, 100 U/ml of penicillin, 10 mg/ml of streptomycin, hygromycin 0.3 mg/ml, G418 0.8 mg/ml. CTL were prepared from OT-I transgenic mouse spleen cell suspensions. RBC were lysed with ACK buffer, and the cell suspension was cultured in an upright T75 flask, in complete RPMI (10% FBS, 50 mM β-ME, 2 mM L-glutamine, 100 U/ml penicillin, and 10 mg/ml streptomycin) plus 10 U/ml IL-2 plus 10 nM OVA peptide for 48–72 h. The cells were washed to remove peptide and resuspended in fresh medium with IL-2. CTL were used from day 5 cultures. For continued culture, after 7–10 days culture and expansion in the presence of IL-2, CD8⁺ cells were restimulated at 7-10d intervals. 1×10⁶ cells/ml were re-stimulated with 3×10⁶ irradiated (3000 rads) B6 spleen cells previously pulsed with 5 µg/ml OVA for 30 min.

Hybridomas expressing the OT-I TCR with or without CD8α and CD8β were made by retroviral transfection of TCR-deficient 58α⁻β⁻ cells⁴⁹. Chimeric genes encoding CD8β-YFP, CD8β-mCherry, CD3ζ-CFP²¹, CD3ζ-eGFP and, Lck-eGFP, Lck-mCherry and CD8α-Lck-Cerulean were constructed, inserted into retroviral vector pBMN-Z (S. Kinoshita and G. Nolan, www.stanford.edu/group/nolan) and were expressed in Plat-E packaging cells. All the mutants were made using the Quickchange Site Mutagenesis Kit (Stratagene). Supernatants of these cells were used to transduce OT-I hybridomas and OT-I CTL. For optimal FRET sensitivity and to avoid false negative results, the acceptor (YFP or mCherry) should be in excess relative to the donor (CFP or eGFP). Clones were selected based on the optimal acceptor/donor molar ratio for FRET; that is, an acceptor/donor molar ratio of 1:1 to 3:1. mCherry-tSH2(ZAP70)³⁶ (Addgene plasmid 27137) was cloned into pBMN-Z vector using Hind-III and Not-I sites. Two different sequences were used for Lck knockdown in pGFP-RS-U6 shRNA vector (#232#ctgcaagacaacctggta and #43# gagaacattgacgtgtgtg). OT-I hybridoma cells were maintained in IMDM medium containing 10% fetal bovine serum (FBS), 2 mM L-glutamine, 100 U/ml penicillin/streptomycin, 50 mM β-mercaptoethanol, 500 µg/ml G418 (selecting for TCRα) and 3 µg/ml puromycin (selecting for TCRβ).

FRET microscopy

A dual-camera system specifically designed for FRET imaging was used for imaging, allowing simultaneous acquisition of donor emission and acceptor emission during donor excitation and fast changes between donor and acceptor excitation. This consisted of two CoolSnapHQ cameras (Roper) attached to a Zeiss 200M microscope through a beam splitter (custom 520LPXR; Chroma) and stationary emission filters. A DG4 galvo illuminator customized with a 300-W xenon lamp (Sutter) was used for rapid wavelength switching. The system was run by Slidebook 6.0 software (3I). The optical filters were as follows (center/bandpass): YFP excitation, 504/12–25 nm; YFP emission, 542/27 nm; CFP excitation, 427/10 nm; CFP emission, 472/30 nm; mCherry excitation, 589/15 nm; mCherry emission, 632/22 nm; Cy5 excitation, 620/52 nm; Cy5 emission, 675/50 nm. Beamsplitting was achieved with a dichroic mirror (Chroma). Exposure times were 0.2–0.5 s, with 2 × 2 binning and a 100X, 1.4 numerical aperture oil objective, and software flatfield correction

was used. Live cells were imaged in HBSS medium supplemented with 1mM CaCl₂, 1mM MgCl₂ and 10 mM HEPES and without antibiotics and were maintained at 37°C by the FCS2 live imaging chamber and objective heater (Bioptechs). APCs were added to a prewarmed imaging chamber coated with poly-D-lysine (Sigma). For fixed-cell imaging, cells were mounted in Slowfade Light antifade mounting media (Molecular Probes).

TIRF microscopy

TIRF microscopy experiments were performed using a 100X 1.45 numerical aperture TIRF objective (Nikon) on a Nikon TE2000U microscope custom modified with a TIRF illumination module. Laser illumination (488 and 561 nm laser lines) were adjusted to impinge on the coverslip at an angle to yield a calculated evanescent field depth (d) < 100 nm. Images were acquired on a 14 bit, cooled charge-coupled device camera (CoolSnap HQ², Roper) controlled through NIS-Elements software (Nikon, Inc.). The images were recorded using 300–500-ms exposures depending on the fluorescence intensity of the sample. In some experiments an Olympus IX83 inverted microscope equipped with a four laser (405, 488, 561 and 647 nm) motorized TIRF module was used and images were obtained in a Hamamatsu ORCA Flash 4.0 camera.

FRET analysis

Crosstalk compensation and extraction of donor-normalized FRET was performed using a 3-filter set algorithm as described previously^{21,30,50}. For each focal position, three exposures were registered: I_{DD} (donor excitation/donor emission), I_{AA} (acceptor excitation/acceptor), and I_{DA} (donor excitation/acceptor, or more generally DA). Background was subtracted based on local fluorescence averaged from a user- specified, cell-free region of each image. The bleed-through coefficients of donor into the DA image and acceptor into the DA image were calibrated using T cells transfected with either CD3 ζ -donor or CD8 β acceptor alone. acceptor>DA bleed-through was $a=12\%$ for eYFP in the dual camera system and $a=7.5\%$ for mCherry in the TIRF system, donor>DA bleed-through was $d=54\%$ for eCFP in the dual camera system and $d=10.6\%$ for eGFP in the TIRF system. Sensitized emission was calculated by simply correcting DA image for donor and acceptor bleedthrough: $F_c = I_{DA} - a * I_{AA} - d * I_{DD}$. To get FRET efficiency (E), we used the following formula: $E_{app} = F_c / (F_c + (G * I_{DD}))$, where G is the independently calibrated ratio of sensitized emission in the I_{DA} filter set before photobleaching, to donor recovery in the I_{DD} filter set after acceptor photobleaching. For eCFP and eYFP in the dual camera system $G=3.83 \pm 0.1$, for eGFP and mCherry in the TIRF system $G=2.1 \pm 0.1$. We have implemented this FRET method as an available upon request ImageJ plug-in modified from Roszik et al.⁵¹. The FRET image was masked to accept only regions in which donor intensity was more than four times above background noise. Cells with donor/acceptor ratios outside the stoichiometric range of 1:1 to 3:1, as well as movement artifacts, were excluded from analysis. The average FRET was calculated from the synapse.

Ca²⁺ flux imaging

H2-K^b-OVA expressing CHO cells were plated in poly-D-lysine coated chambers then, after washing in Ca²⁺/Mg²⁺ free medium containing 1 mM EGTA, OT-I T cell hybridoma cells

expressing both CD8 α and CD8 β loaded with 2 μ M Ca²⁺ sensitive dye Fluo-4 were added on top. Imaging of Fluo-4 fluorescence was conducted in HBSS supplemented with 2.5 mM CaCl₂, 2.5 mM MgCl₂ and 10 mM HEPES. In the case of primary cells, Fluo-4 loaded CTLs were added to lipid bilayers containing the appropriate antigen, after allowing cells to settle in Ca²⁺/Mg²⁺ free medium containing 1 mM EGTA, 1 volume of pre-warmed HBSS supplemented with 2.5 mM CaCl₂, 2.5 mM MgCl₂ and 10 mM HEPES was added.

Determination of molecular density on cell surface and Adhesion Frequency Assay

For every micropipette experiment, site densities of MHCp on RBCs and TCR and CD8 on T cells were measured by flow cytometry. To measure the MHCp site density, RBCs were incubated with PE-conjugated mAb 3H2672 (for H-2K^b) at 10 μ g/ml in 200 μ l of FACS buffer (RPMI 1640, 5 mM EDTA, 1% BSA and 0.02% sodium azide) on ice for 40 min. Similarly, CD8 α subunit (clone 53–6.7), CD8 β subunit (clone H35-17.2), TCR V α 2 (clone B20.1), and CD3 ϵ (clone 145-2-C11) expressed on T cells were stained with their respective PE-conjugated mAbs (1:300 dilution, eBiosciences). CD8 is expressed as either an $\alpha\alpha$ homodimer or an $\alpha\beta$ heterodimer. Therefore, it is assumed that the site density of CD8 $\alpha\beta$ equals that of CD8 β whereas the site density of CD8 $\alpha\alpha$ equals half of the site density difference between CD8 α and CD8 β .

For the adhesion frequency assay³⁵, an OT-I T cell and a RBC were aspirated by respective pipettes and driven in and out of contact with controlled area and duration. Adhesion was observed from stretching of the RBC on T cell retraction. This contact-retraction cycle was either repeated 50 times for a given contact duration on each cell pair, and 3–5 cell pairs were used to estimate an adhesion frequency P_a (mean \pm SEM). P_a can be converted to the average number $\langle n \rangle$ by $\langle n \rangle = 1 - \ln(1 - P_a)$ and divided by ligand density m_{pMHC} to obtain normalized adhesion bonds $\langle n \rangle / m_{pMHC}$. Experiments were performed at room temperature.

Liposomes and Lipid bilayer preparation

1,2-dioleoyl-sn-glycero-3-phosphocholine (DOPC) was mixed in chloroform with 0.2 mol % 1,2-dioleoyl-sn-glycero-3-[(N-(5- amino-1-carboxypentyl) iminodiacetic acid)succinyl] (Ni-NTA-DOGS) and 0.2 mol% 1,2-dioleoyl-sn-glycero-3-phosphoethanolamine-N-Cap-Biotinyl (CAP-biotin-PE), all the lipids were from Avanti Polar Lipids, dried under vacuum and sonicated in 2% OG. The liposome solution was then extruded through a 0.22 μ m filter and dialyzed against 4l of Tris saline buffer (Tris HCl 20 mM, NaCl 50 mM). Glass slides (No 1, 24 mm \times 50 mm German borosilicate; Menzel-Gläser) were treated with Piranha solution (70% sulfuric acid and 30% hydrogen peroxide) (both from Sigma-Aldrich) for 20 min, rinsed with doubly distilled or deionized water, dried in air and attached with epoxy glue to the bottom of 8-well LabTek II chambers (Nunc), from which the glass bottom had been removed. Slides were exposed to a tenfold diluted lipid suspension for 10 min and rinsed with HEPES-Na buffer (150 mM NaCl, 5 mM HEPES [pH 7.4]). 0.25 mM NiSO₄ was introduced into the chamber for 10 min to charge NTA- DOGS with Ni²⁺. Lipid bilayers was then blocked with blocking buffer (5 mg/ml BSA in HEPES-Na buffer [pH 7.4]) in the presence of 1 μ g/ml His-tagged ICAM-1 for 30 min. The blocked bilayer was incubated sequentially with 1 μ g/ml streptavidin for 30 min followed by 1 μ g/ml H2-K^b-

peptide for 1h. After washing, the bilayers were imaged in HBSS supplemented with 1 mM CaCl₂, 1 mM MgCl₂ and 10 mM HEPES.

Immunoblots

Cells (5×10⁶) were lysed in 1% Brij96, 50 mM HEPES, pH 7.4, 150 mM NaCl, 1 mM Na₃VO₄, 1 mM PMSF and a protease inhibitor ‘cocktail’ were separated by 10% reducing SDS-PAGE, blotted, and incubated with specific primary antibodies followed by incubation with goat anti-rabbit IgG (HIL), DyLight 800-conjugated (Pierce, #35571) or goat anti-mouse IgG (HIL), DyLight 680-conjugated (Pierce, #35519), and detected and quantified with a LiCor Odyssey infrared imaging system.

Colocalization analysis

This was performed with JACoP plugin in ImageJ. Background levels were obtained by measuring the mean intensity of each signal outside the cells and were subtracted; negative pixel values were clipped to zero. Pearson’s *P* colocalization index were calculated.

Supplementary Material

Refer to Web version on PubMed Central for supplementary material.

Acknowledgments

We thank Kersi Pestonjamas for technical help, Lorena García and Joaquín Sebastián for their critical reading and the NIH Tetramer Core Facility for production of biotinylated MHC I proteins and tetramers. Supported by National University of Singapore and NIH grants GM065230 to N.R.J.G. and GM96187 and AI038282 to C.Z. J.A.H.H. was supported by NIH training grant T32AI07244. R.Z. is supported by Investigator Award 096669 from the Wellcome Trust. The content is solely the responsibility of the authors and does not necessarily represent the official views of the National Institute of General Medical Sciences, the National Institutes of Health, or other funding agencies. This is manuscript number 27062 from The Scripps Research Institute.

References

1. Acuto O, Di Bartolo V, Michel F. Tailoring T-cell receptor signals by proximal negative feedback mechanisms. *Nat Rev Immunol.* 2008; 8:699–712. [PubMed: 18728635]
2. Salmond RJ, Filby A, Qureshi I, Caserta S, Zamoyska R. T-cell receptor proximal signaling via the Src-family kinases, Lck and Fyn, influences T-cell activation, differentiation, and tolerance. *Immunol Rev.* 2009; 228:9–22. [PubMed: 19290918]
3. Gascoigne NRJ, Casas J, Brzostek J, Rybakin V. Initiation of TCR Phosphorylation and Signal Transduction. *Front Immun.* 2011; 2
4. Artyomov MN, Lis M, Devadas S, Davis MM, Chakraborty AK. CD4 and CD8 binding to MHC molecules primarily acts to enhance Lck delivery. *Proc Natl Acad Sci USA.* 2010; 107:16916–16921. [PubMed: 20837541]
5. Pitcher LA, et al. The formation and functions of the 21- and 23-kDa tyrosine-phosphorylated TCR ζ subunits. *Immunol Rev.* 2003; 191:47–61. [PubMed: 12614351]
6. Zamoyska R, et al. The influence of the src-family kinases, Lck and Fyn, on T cell differentiation, survival and activation. *Immunol Rev.* 2003; 191:107–118. [PubMed: 12614355]
7. Fooksman DR, et al. Functional Anatomy of T Cell Activation and Synapse Formation. *Annu Rev Immunol.* 2010; 28:79–105. [PubMed: 19968559]
8. Huse M, et al. Spatial and Temporal Dynamics of T Cell Receptor Signaling with a Photoactivatable Agonist. *Immunity.* 2007; 27:76–88. [PubMed: 17629516]

9. Jiang N, et al. Two-Stage Cooperative T Cell Receptor-Peptide Major Histocompatibility Complex-CD8 Trimolecular Interactions Amplify Antigen Discrimination. *Immunity*. 2011; 34:13–23. [PubMed: 21256056]
10. Holler PD, Kranz DM. Quantitative analysis of the contribution of TCR/pepMHC affinity and CD8 to T cell activation. *Immunity*. 2003; 18:255–264. [PubMed: 12594952]
11. Wooldridge L, et al. Interaction between the CD8 coreceptor and major histocompatibility complex class I stabilizes T cell receptor-antigen complexes at the cell surface. *J Biol Chem*. 2005; 280:27491–27501. [PubMed: 15837791]
12. Boggon TJ, Eck MJ. Structure and regulation of Src family kinases. *Oncogene*. 2004; 23:7918–7927. [PubMed: 15489910]
13. Ehrlich LIR, Ebert PJR, Krummel MF, Weiss A, Davis MM. Dynamics of p56lck Translocation to the T Cell Immunological Synapse following Agonist and Antagonist Stimulation. *Immunity*. 2002; 17:809–822. [PubMed: 12479826]
14. Kim PW, Sun ZYJ, Blacklow SC, Wagner G, Eck MJ. A zinc clasp structure tethers Lck to T cell coreceptors CD4 and CD8. *Science*. 2003; 301:1725–1728. [PubMed: 14500983]
15. Nika K, et al. Constitutively Active Lck Kinase in T Cells Drives Antigen Receptor Signal Transduction. *Immunity*. 2010; 32:766–777. [PubMed: 20541955]
16. Rossy J, Williamson DJ, Gaus K. How does the kinase Lck phosphorylate the T cell receptor? Spatial organization as a regulatory mechanism. *Front Immun*. 2012; 3
17. van der Merwe PA, Cordoba SP. Late arrival: recruiting coreceptors to the T cell receptor complex. *Immunity*. 2011; 34:1–3. [PubMed: 21272780]
18. Xu H, Littman DR. A kinase-independent function of Lck in potentiating antigen-specific T cell activation. *Cell*. 1993; 74:633–643. [PubMed: 8358792]
19. Lee-Fruman KK, Collins TL, Burakoff SJ. Role of the Lck Src homology 2 and 3 domains in protein tyrosine phosphorylation. *J Biol Chem*. 1996; 271:25003–25010. [PubMed: 8798782]
20. Fragoso RC, Pyarajan S, Irie HY, Burakoff SJ. A CD8/Lck transgene is able to drive thymocyte differentiation. *J Immunol*. 2006; 177:6007–6017. [PubMed: 17056525]
21. Zal T, Zal MA, Gascoigne NRJ. Inhibition of T cell receptor-coreceptor interactions by antagonist ligands visualized by live FRET imaging of the T-hybridoma immunological synapse. *Immunity*. 2002; 16:521–534. [PubMed: 11970876]
22. Gascoigne NRJ, Zal T. Molecular interactions at the T cell-antigen-presenting cell interface. *Curr Opin Immunol*. 2004; 16:114–119. [PubMed: 14734119]
23. Yachi PP, Ampudia J, Gascoigne NRJ, Zal T. Nonstimulatory peptides contribute to antigen-induced CD8–T cell receptor interaction at the immunological synapse. *Nature Publishing Group*. 2005; 6:785–792.
24. Yachi PP, Ampudia J, Zal T, Gascoigne NRJ. Altered Peptide Ligands Induce Delayed CD8-T Cell Receptor Interaction—a Role for CD8 in Distinguishing Antigen Quality. *Immunity*. 2006; 25:203–211. [PubMed: 16872849]
25. Mallaun M, et al. The T cell receptor’s alpha-chain connecting peptide motif promotes close approximation of the CD8 coreceptor allowing efficient signal initiation. *J Immunol*. 2008; 180:8211–8221. [PubMed: 18523287]
26. Grakoui A, et al. The immunological synapse: a molecular machine controlling T cell activation. *Science*. 1999; 285:221–227. [PubMed: 10398592]
27. Hoerter JAH, et al. Coreceptor affinity for MHC defines peptide specificity requirements for TCR interaction with coagonist peptide-MHC. *Journal of Experimental Medicine*. 2013; 210:1807–1821. [PubMed: 23940257]
28. Rybakin V, Clamme J-P, Ampudia J, Yachi PP, Gascoigne NRJ. CD8 $\alpha\alpha$ and- $\alpha\beta$ isotypes are equally recruited to the immunological synapse through their ability to bind to MHC class I. *EMBO Rep*. 2011; 10.1038/embor.2011.209
29. Förster T. Energy migration and fluorescence. 1946. *J Biomed Opt*. 2012; 17:011002. [PubMed: 22352636]
30. Zal T, Gascoigne NRJ. Photobleaching-corrected FRET efficiency imaging of live cells. *Biophysical Journal*. 2004; 86:3923–3939. [PubMed: 15189889]

31. Groves JT, Dustin ML. Supported planar bilayers in studies on immune cell adhesion and communication. *J Immunol Methods*. 2003; 278:19–32. [PubMed: 12957393]
32. Devine L, et al. Mapping the binding site on CD8 beta for MHC class I reveals mutants with enhanced binding. *J Immunol*. 2006; 177:3930–3938. [PubMed: 16951356]
33. Zamoyska R, et al. Inability of CD8 alpha' polypeptides to associate with p56lck correlates with impaired function in vitro and lack of expression in vivo. *Nature*. 1989; 342:278–281. [PubMed: 2509945]
34. Huang J, Edwards LJ, Evavold BD, Zhu C. Kinetics of MHC-CD8 interaction at the T cell membrane. *J Immunol*. 2007; 179:7653–7662. [PubMed: 18025211]
35. Chesla SE, Selvaraj P, Zhu C. Measuring two-dimensional receptor-ligand binding kinetics by micropipette. *Biophysical Journal*. 1998; 75:1553–1572. [PubMed: 9726957]
36. Yudushkin IA, Vale RD. Imaging T-cell receptor activation reveals accumulation of tyrosine-phosphorylated CD3 ζ in the endosomal compartment. *Proc Natl Acad Sci USA*. 2010; 107:22128–22133. [PubMed: 21135224]
37. Iwashima M, Irving BA, van Oers NS, Chan AC, Weiss A. Sequential interactions of the TCR with two distinct cytoplasmic tyrosine kinases. *Science*. 1994; 263:1136–1139. [PubMed: 7509083]
38. van Oers NS, Killeen N, Weiss A. Lck regulates the tyrosine phosphorylation of the T cell receptor subunits and ZAP-70 in murine thymocytes. *J Exp Med*. 1996; 183:1053–1062. [PubMed: 8642247]
39. Au-Yeung BB, et al. The structure, regulation, and function of ZAP-70. *Immunol Rev*. 2009; 228:41–57. [PubMed: 19290920]
40. Palacios EH, Weiss A. Function of the Src-family kinases, Lck and Fyn, in T-cell development and activation. *Oncogene*. 2004; 23:7990–8000. [PubMed: 15489916]
41. Legname G, et al. Inducible expression of a p56Lck transgene reveals a central role for Lck in the differentiation of CD4 SP thymocytes. *Immunity*. 2000; 12:537–546. [PubMed: 10843386]
42. Seddon B. Long-Term Survival But Impaired Homeostatic Proliferation of Naive T Cells in the Absence of p56lck. *Science*. 2000; 290:127–131. [PubMed: 11021796]
43. Levin SD, Abraham KM, Anderson SJ, Forbush KA, Perlmutter RM. The protein tyrosine kinase p56lck regulates thymocyte development independently of its interaction with CD4 and CD8 coreceptors [corrected]. 1993;245–255.10.1084/jem.178.1.245
44. Yamaguchi H, Hendrickson WA. Structural basis for activation of human lymphocyte kinase Lck upon tyrosine phosphorylation. *Nature*. 1996; 384:484–489. [PubMed: 8945479]
45. Paster W, et al. Genetically encoded Förster resonance energy transfer sensors for the conformation of the Src family kinase Lck. *The Journal of Immunology*. 2009; 182:2160–2167. [PubMed: 19201869]
46. Stirnweiss A, et al. T Cell Activation Results in Conformational Changes in the Src Family Kinase Lck to Induce Its Activation. *Science signaling*. 2013; 6:ra13–ra13. [PubMed: 23423439]
47. Thome M, Duplay P, Guttinger M, Acuto O. Syk and ZAP-70 mediate recruitment of p56lck/CD4 to the activated T cell receptor/CD3/zeta complex. *J Exp Med*. 1995; 181:1997–2006. [PubMed: 7539035]
48. Thome M, Germain V, DiSanto JP, Acuto O. The p56lck SH2 domain mediates recruitment of CD8/p56lck to the activated T cell receptor/CD3/zeta complex. *Eur J Immunol*. 1996; 26:2093–2100. [PubMed: 8814252]
49. Stotz SH, Bolliger L, Carbone FR, Palmer E. T cell receptor (TCR) antagonism without a negative signal: evidence from T cell hybridomas expressing two independent TCRs. *J Exp Med*. 1999; 189:253–264. [PubMed: 9892608]
50. Zal T, Gascoigne NRJ. Using live FRET imaging to reveal early protein-protein interactions during T cell activation. *Curr Opin Immunol*. 2004; 16:418–427. [PubMed: 15245734]
51. Roszik J, Lisboa D, Szöllösi J, Vereb G. Evaluation of intensity-based ratiometric FRET in image cytometry--approaches and a software solution. *Cytometry A*. 2009; 75:761–767. [PubMed: 19591240]

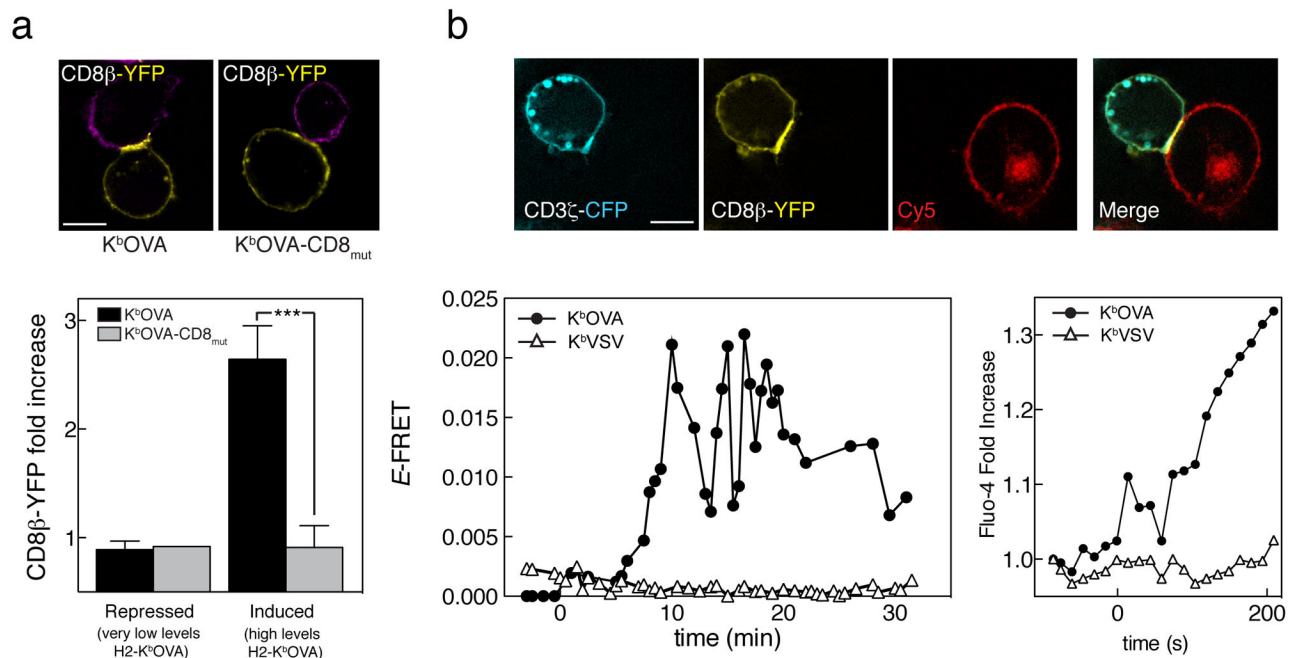


Figure 1. Recruitment of CD8 and imaging of the induction of TCR-CD8 FRET by agonist
 (a) OT-I hybridomas expressing CD8 α wild-type, CD3 ζ -CFP, and CD8 β -YFP (OT-I.ZC.8 β Y) were incubated with Cy5-stained CHO cells expressing tetracycline-induced wild-type single-chain H2-K^bOVA (left) or a mutant that cannot bind to CD8 (right). The image of each panel shows mid-cell sections of fluorescence images (CD8 β -YFP in yellow and Cy5 in purple). Scale bar 5 μ m. The bottom graph shows the quantitation of CD8 β -YFP recruitment to the immune synapse when scH2-K^b-OVA (black) or scH2-K^b-CD8_{mut}-OVA (grey) was expressed on CHO cells surface. Mean fluorescence intensity \pm s.e.m., n=25 conjugates. Unpaired t-test * p<0.0001. (b) Top row shows a representative image of OT-I.ZC.8 β Y cells forming the immune synapse formation (CD3 ζ -CFP in cyan, CD8 β -YFP in yellow and CHO APC membrane labeled with Cy3.5 in red). Bottom left plot shows live FRET efficiency of OT-I.ZC.8 β Y cells incubated with scH2-K^b-OVA (closed circles) or – VSV (open triangles) expressing CHO cells. Data represent average FRET efficiency at the synapse. Bottom right panel shows Ca²⁺ flux from a Fluo-4 loaded OT-I cell expressing CD8 α /CD8 β during interaction with a CHO cell expressing scH2-K^b-OVA (circles) or – VSV (triangles). The results are representative of at least three independent experiments.

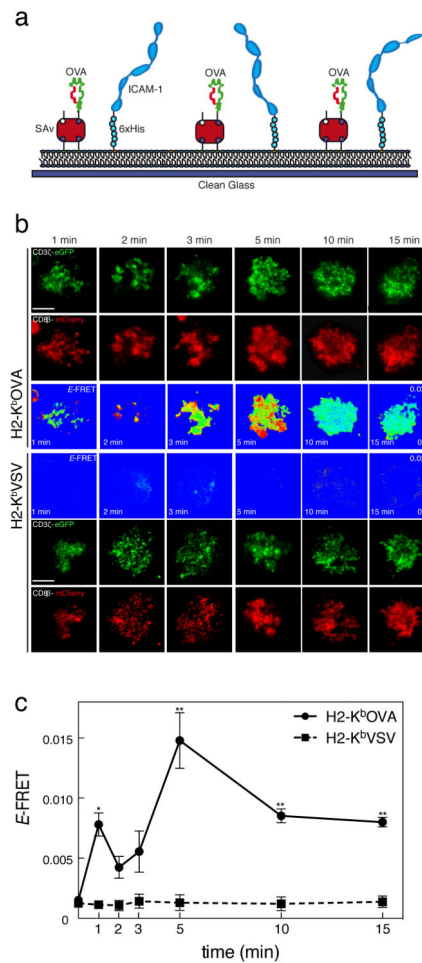


Figure 2. Induction of TCR-CD8 FRET by agonist on artificial lipid bilayers

(a) Scheme of artificial lipid bilayers artificial based APC. (b) OT-I hybridomas expressing CD8 α wild-type, CD3 ζ -eGFP, and CD8 β -mCherry (OT-I.ZG.8 β R) were added to lipid bilayers containing either H2-K^b-OVA or H2-K^b-VSV monomers and ICAM-1, fixed at the indicated time points and imaged by TIRFM at the immune synapses. Images shown in green represent CD3 ζ -eGFP, CD8 β -mCherry in red and FRET efficiency in false color scale. Images are representative of three different experiments. Scale bar 5 μ m. (c) FRET efficiency analysis of immune synapses from OT-I.ZG.8 β R interacting with lipid bilayers containing H2-K^b-OVA (circles). Mean \pm s.e.m. of 1 min n=18, 2 min n=33, 3 min n=18, 5 min n=45, 10 min n=50 and 15 min n=52. Or H2-K^b-VSV bilayers (squares), mean \pm s.e.m. of 1 min n=12, 2 min n=15, 3 min n=13, 5 min n=21, 10 min n=14 and 15 min n=13. Unpaired t-test. *p<0.01 and **p<0.001.

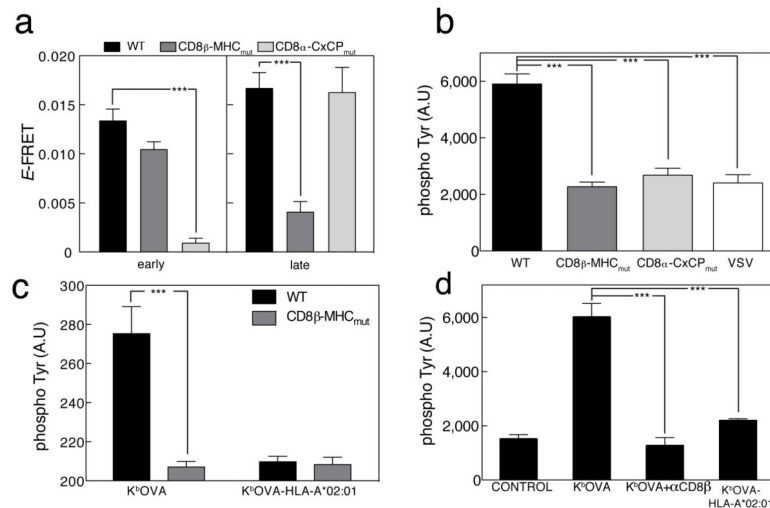


Figure 3. Two stage interaction between TCR-CD8

(a) OT-I hybridomas expressing CD8 α WT, CD3 ζ -eGFP, and CD8 β -mCherry (black); CD8 α WT, CD3 ζ -eGFP, and CD8 β -MHC_{mut}-mCherry (dark grey) or CD8 α -CxCP_{mut}, CD3 ζ -eGFP, and CD8 β -mCherry (light grey) were added to lipid bilayers containing K^b-OVA and ICAM-1, fixed at 1 min (“early”) or 10 min (“late”), and imaged by TIRFM at the immune synapses. FRET efficiency \pm s.e.m. was plotted, “early” WT (n=30), CxCP_{mut} (n=25), MHC_{mut} (n=28), and “late” n=28, 24, 29, respectively. (b) OT-I hybridomas expressing CD8 $\alpha\beta$ WT (black); CD8 $\alpha\beta$ -MHC_{mut} (dark gray) or CD8 α -CxCP_{mut} and CD8 β WT (light gray) were stimulated as in (a) for 15 min and stained with anti-phospho-Tyr. Images were taken using TIRFM. Mean fluorescence of WT n=20, MHC_{mut} n=33, CxCP_{mut} n=36 and VSV n=21 \pm s.e.m. is shown. OT-I cells expressing CD8 $\alpha\beta$ -WT (white) were added to bilayers containing K^b-VSV and ICAM-1 as a negative control. (c) OT-I hybridomas expressing CD8 $\alpha\beta$ -WT (black) or CD8 $\alpha\beta$ -MHC_{mut} (dark gray) were added to bilayers containing either K^b-OVA or K^b-OVA-HLA-A*02:01 plus ICAM-1 for 15 min, then stained with anti-phospho-Tyr. Mean fluorescence \pm s.e.m. shown for K^b-OVA, WT n=15; CD8 β -MHC_{mut} n=15 and for K^b-OVA-HLA-A*02:01 WT n=15; CD8 β -MHC_{mut} n=19. (d) Primary mouse OT-I CTL were pretreated with blocking anti-CD8 (dark gray) or directly (black) added to bilayers containing either K^b-OVA or K^b-OVA-HLA-A*02:01 plus ICAM-1 or ICAM-1 alone (control) for 15 min, then stained with anti-phospho-Tyr. Mean fluorescence of control n=23, K^b-OVA n=17, anti-CD8 β n=19 and K^b-OVA-HLA-A*02:01 n=20 \pm s.e.m. are shown. Unpaired t-test. ***p<0.0001.

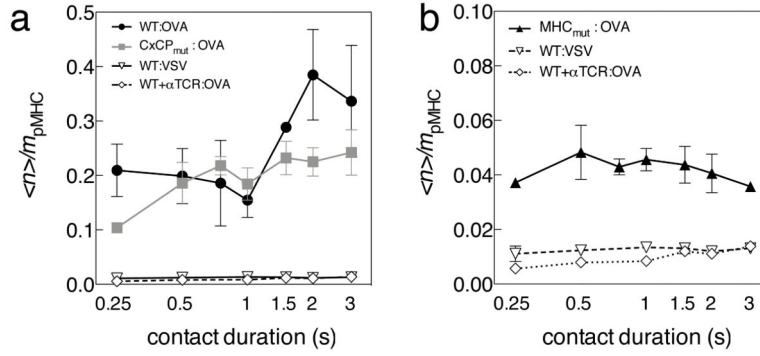


Figure 4. Adhesion Frequency Assay

(a) Frequency of adhesion was normalized to the amount of pMHC presented ($\langle n \rangle / m_{pMHC}$) and plotted against time t for OT-I hybridomas expressing CD8 α wild-type and CD8 β -wild-type (closed circles); or CD8 α -CxCP_{mut} and CD8 β wild-type (closed squares) T cells interacting with RBCs bearing 4 and 7 OVA:H-2K^b/mm² respectively at 37°C. Controls with CD8-wild-type cells pretreated with a blocking antibody against TCR (open diamond), or using RBCs bearing 93 VSV:H-2K^b/mm² (open triangle) were conducted. Representative data from three repeated experiments are shown. (b) $\langle n \rangle / m_{pMHC}$ versus t data of OT-I hybridomas expressing CD8 α wild-type and CD8 β -MHC_{mut} (closed triangles) T cells interacting with RBCs bearing 23 OVA:H-2K^b/μm². Controls with CD8-wild-type cells pretreated with a blocking antibody against TCR (open diamond), or using RBCs bearing 93 VSV:H-2K^b/mm² (open triangle) were conducted. Data are representative of three experiments.

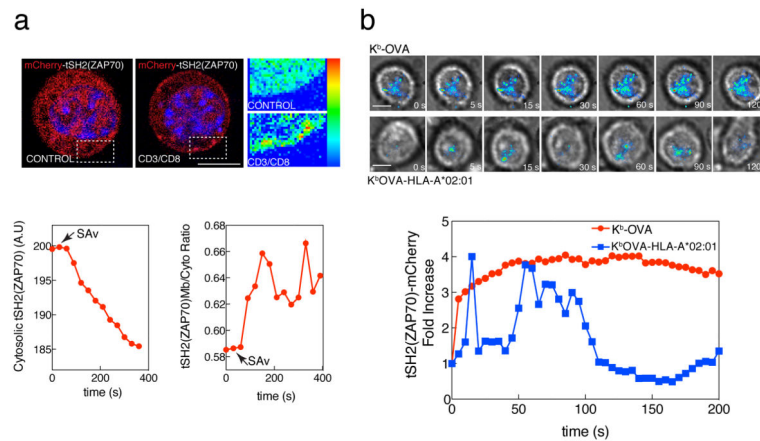


Figure 5. CD8/MHCp interaction is required for sustained signaling through the TCR
 (a) Nuclei of OT-I primary CTL expressing mCherry-tSH2(ZAP70) were stained with the live cell imaging-compatible Hoechst 33342 and then incubated with a mixture of biotinylated anti-CD3 ϵ and anti-CD8 β antibodies and imaged under a deconvolution microscope. Top row shows the localization of mCherry-tSH2(ZAP70) before (left) and after the addition of crosslinking streptavidin (right). Higher detail in zoomed boxes in false color. Bottom, graphs showing decrease in cytosolic fluorescence after streptavidin addition (left) in selected regions, or ratio between membrane/cytosolic fluorescence (right). Data are representative of at least three different experiments. Scale bar 5 μ m. (b) OT-I primary CTL cells expressing mCherry-tSH2(ZAP70) were added to lipid bilayers containing either H2-K^b-OVA or H2-K^b-OVA-HLA-A*02:01 monomers and ICAM-1, and analyzed by live cell TIRFM at the immune synapses. Representative time points are shown in the top rows where the cells can be seen by transmitted light and the recruitment of mCherry-tSH2(ZAP70) is shown as false color overlaid image. Bottom graph, normalized mean mCherry-tSH2(ZAP70) fluorescence at the immune synapse in bilayers containing either H2-K^b-OVA (red) or H2-K^b-OVA-HLA-A*02:01 (blue). Data are representative of three experiments.

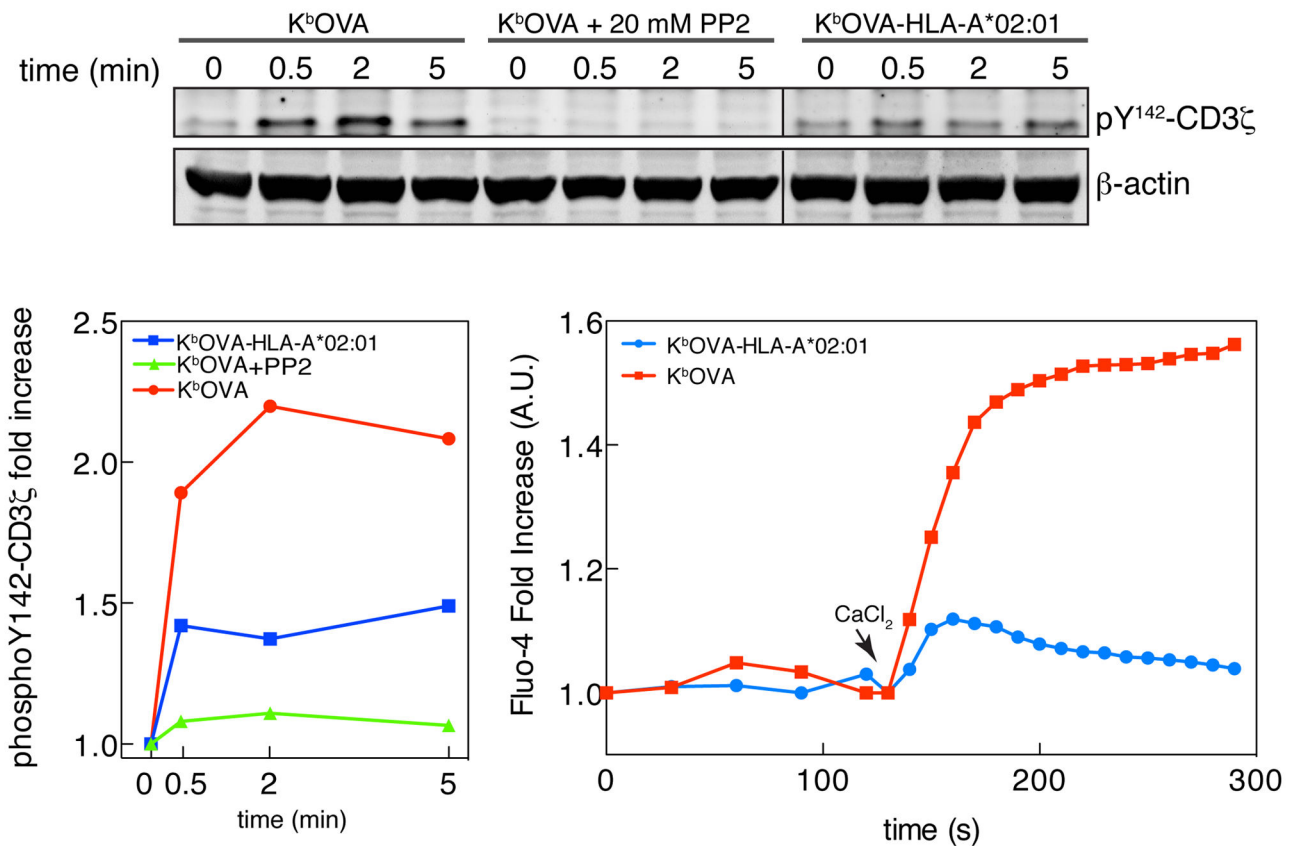


Figure 6. Src kinase family activity is responsible of TCR phosphorylation after antigen recognition

Primary OT-I CTL were pretreated or not with the general Src kinase inhibitor PP2 (20 mM) and then stimulated with either H2-K^b-OVA or H2-K^b-OVA-HLA-A*02:01 tetramers for the indicated times. CD3ζ phosphorylation was analyzed by immunoblot. Quantitation of band intensities is shown in the left plot. In the right-hand plot, cells were loaded with Ca²⁺ sensitive dye Fluo-4 and imaged after the addition on top of bilayers containing either H2-K^b-OVA or H2-K^b-OVA-HLA-A*02:01 monomers plus ICAM-1, as described in methods section. Data are representative of four experiments. Data are representative of three experiments.

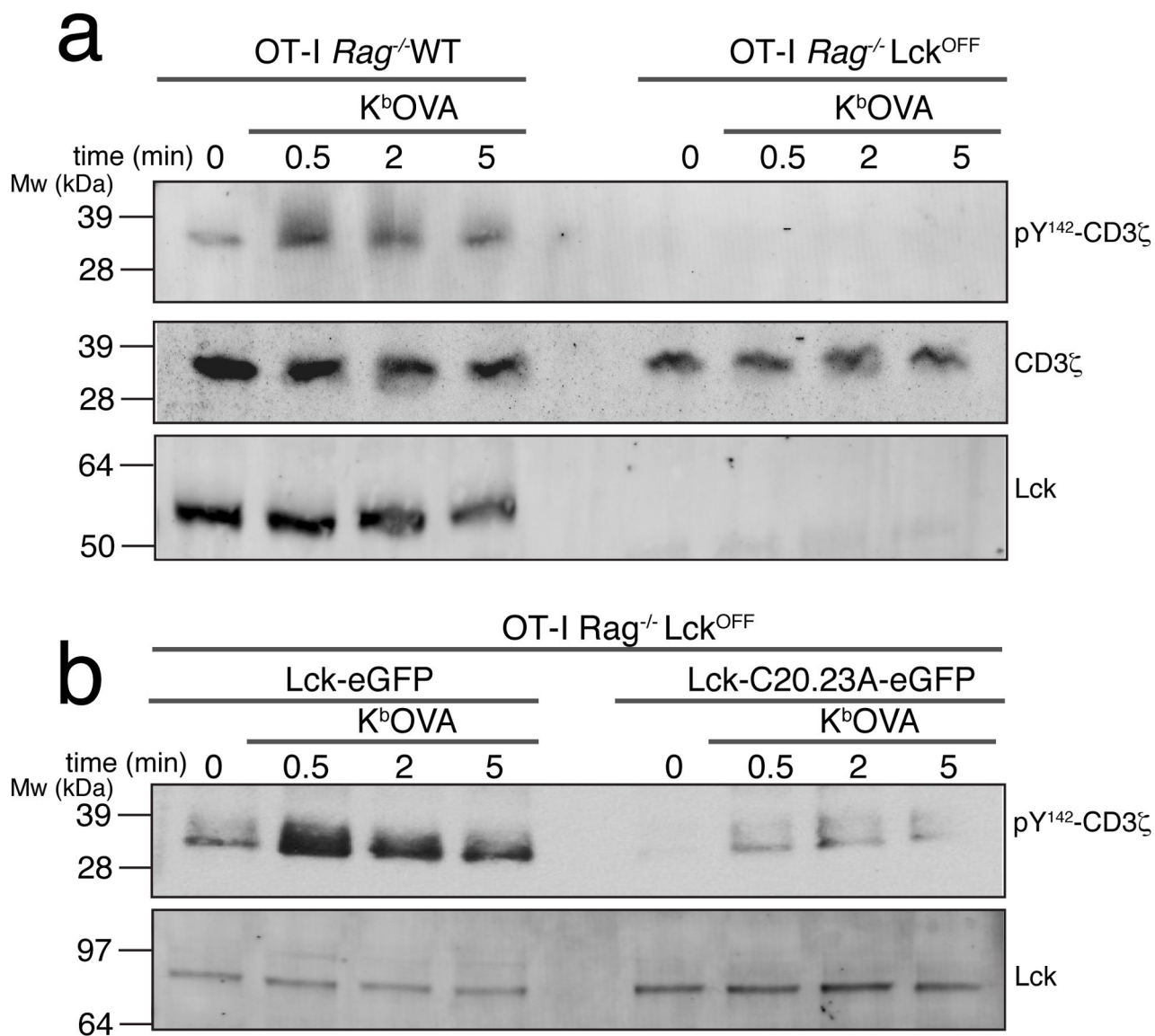


Figure 7. Free Lck is responsible for initial TCR phosphorylation

(a) OT-I *Rag*^{-/-} wild-type or Lck^{OFF} CTL were stimulated with H2-K^b-OVA tetramers for the indicated times. CD3 ζ phosphorylation and Lck expression were analyzed by immunoblot. Data are representative of three experiments. (b) OT-I *Rag*^{-/-} Lck^{OFF} CTL cells were transduced with Lck-eGFP wild-type or with the mutant Lck(C20.23A)-eGFP and then stimulated with H2-K^b-OVA tetramers for the indicated times. CD3 ζ phosphorylation and total Lck expression was analyzed by immunoblot. Data are representative of two experiments.

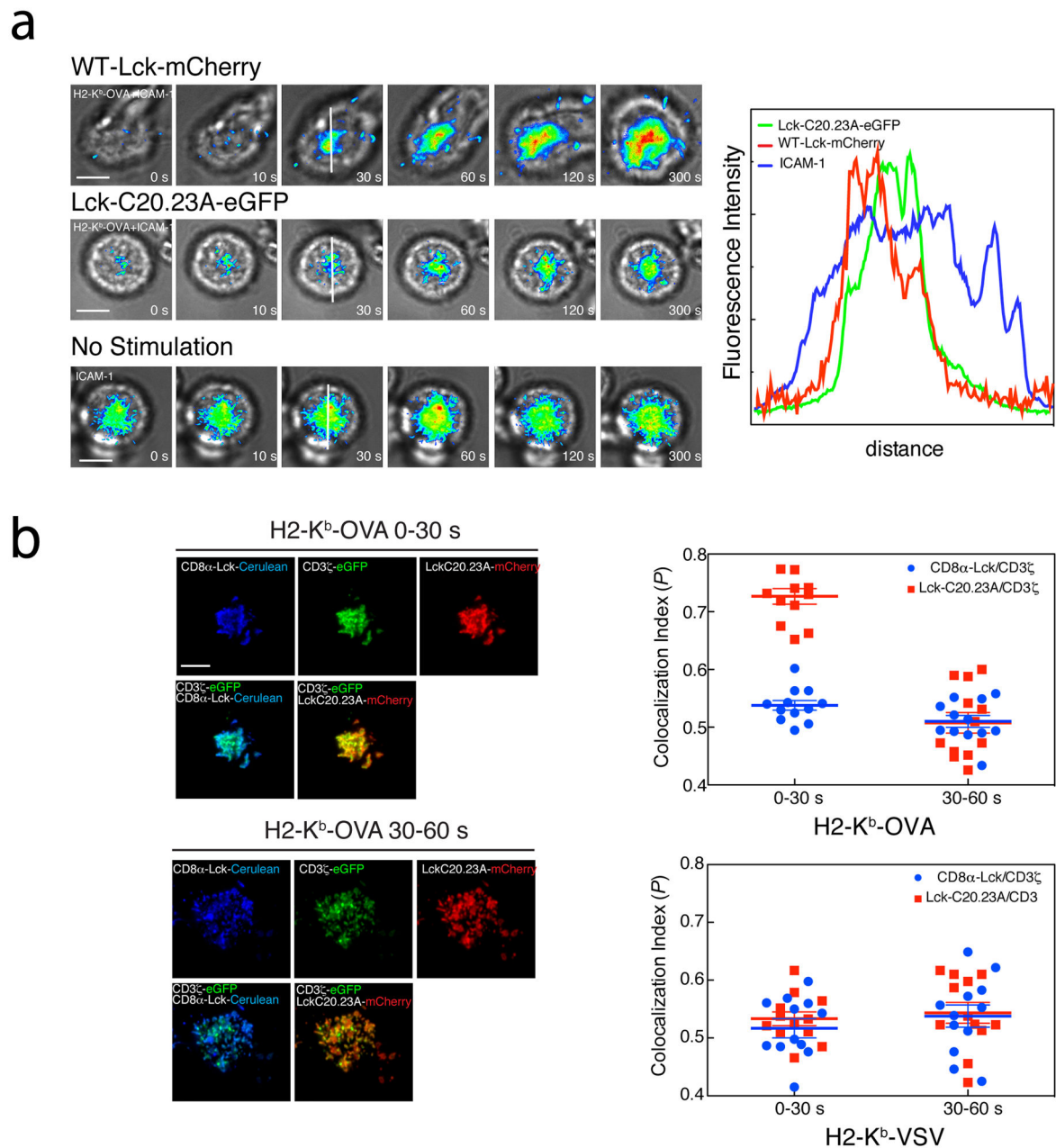


Figure 8. Lck recruitment analysis

(a) OT-I *Rag1*^{-/-} CTL were transduced with wild-type mCherry fused Lck (top row) or mutant LckC20.23A-eGFP (middle row), added to lipid bilayers containing H2-K^b-OVA monomers and ICAM-1 (top two rows), or ICAM-1 only (bottom row), and the immune synapses were imaged under TIRF microscopy. Cells can be followed by transmitted light. Lck intensity is shown in false color at selected time points. Scale bar 5 μ m. Bottom, intensity line profile of cell interacting with bilayers containing H2-K^b-OVA monomers and ICAM-1 (green) or ICAM-1 only (blue). Data are representative of three experiments. (b) Double colocalization analysis of immune synapses from OT-I.ZG.8 α LckC.8 β .Lck

C2023A.R cells interacting with lipid bilayers containing H2-K^b-OVA (left) or H2-K^b-VSV(right) plus ICAM-1. Scale bar 5 μ m. Means \pm s.e.m. of two separate experiments of Pearson's coefficient between CD3 ζ -eGFP and Lck-C20.23A-mCherry (red squares) or CD3 ζ -eGFP and CD8 α -Lck-Cerulean (blue circles) were plotted.

Author Manuscript

Author Manuscript

Author Manuscript

Author Manuscript